ORIGINAL RESEARCH



Adaptive second order sliding mode control of an oscillating water column

Facundo D. Mosquera¹ | Carolina A. Evangelista¹ | Paul F. Puleston¹ | John V. Ringwood²

¹LEICI Institute, National University of La Plata-CONICET, La Plata, Argentina

²Centre for Ocean Energy Research (COER), Maynooth University, Maynooth, Ireland

Correspondence

John V. Ringwood, Centre for Ocean Energy Research (COER), Maynooth University, Maynooth, Ireland.

Email: john.ringwood@mu.ie

Funding information

Science Foundation Ireland, Grant/Award Number: 12/RC/2302_P2; Agencia Nacional de Promoción de la Investigación, el Desarrollo Tecnológico y la Innovación; Universidad Nacional de La Plata, Grant/Award Number: Facultad de Ingeniería

Abstract

The energy from waves has a vast untapped potential to contribute to renewable energy supply and diversification. For that reason, wave energy conversion systems have been a topical research area in recent years. In particular, harnessing wave energy with an oscillating water column converter has proved to be one suitable solution, which has also seen a number of successful deployments. Nevertheless, additional research is required for this technology in order to reach full commercial maturity and economic performance. This paper proposes an adaptive second order sliding mode controller to maximise the converted energy. In particular, the proposed adaptive control setup maintains the sliding mode robust features, while reducing high frequency oscillations and abrupt control actions produced by fixed-gain algorithms. A comparison of energy generation performance shows better energy conversion efficiency of the proposed control strategy over standard speed regulation control strategies, even considering air compression dynamics and hydrodynamics in the tests.

1 | INTRODUCTION

Around the world, research and development of wave energy converters (WECs) is accelerating, as the need for diverse renewable energy sources grows [1–3]. Many WEC devices, including the popular oscillating water column (OWC) WEC, are being tested at sea or deployed for commercial trial [4, 5]. A breakwater-mounted OWC system is shown in Figure 1.

Maximizing power production is a critical component in the drive to make wave energy cost-effective [2]. However, this is a challenging task due to the significant variability of the wave-generated airflow over time, the nonlinear nature of WECs, and their inherent uncertainties and external disturbances. A suitable control system can successfully address these challenges [1, 6].

Advanced control techniques have been proposed for OWC-WECs over the past three decades [7], with a main focus on maximizing power extraction through speed control of the electric generator [7–11]. Some of these techniques include first order sliding mode control (SMC) [12–14], which has proven to be a powerful design tool for synthesizing robust finite-

time convergence controllers for nonlinear systems, particularly in uncertain electromechanical applications [15–17]. However, classical first order SMC can result in a significant amount of chattering, an undesired phenomenon characterized by finite-frequency and finite-amplitude oscillations due to the use of discontinuous control action applied to the first time derivative of the sliding variable [18].

To reduce chattering, several innovative solutions have been proposed over the years. Some approaches are boundary layer control, that is, replacing the discontinuous sign(·) terms in the control function by piece-wise linear or smooth approximations of the switching [19, 20], observer based SMC, that is, localize the the high frequency phenomena in the feedback loop by combining discontinuous control which an asymptotic observer [21], and others [22–24]. Among these, SOSM control is one of the most successful and widespread approaches to reducing chattering [18, 25–27]. In SOSM techniques, the discontinuous action is applied to the second time derivative of the sliding variable, providing a smoother control signal than that obtained via first order SMC. This control action is advantageous for the lifespan of the actuators [18, 28, 29].

This is an open access article under the terms of the Creative Commons Attribution License, which permits use, distribution and reproduction in any medium, provided the original work is properly cited.

© 2023 The Authors. IET Renewable Power Generation published by John Wiley & Sons Ltd on behalf of The Institution of Engineering and Technology.

5 wileyonlinelibrary.com/iet-rpg IET Renew. Power Gener. 2024;18:226–237.

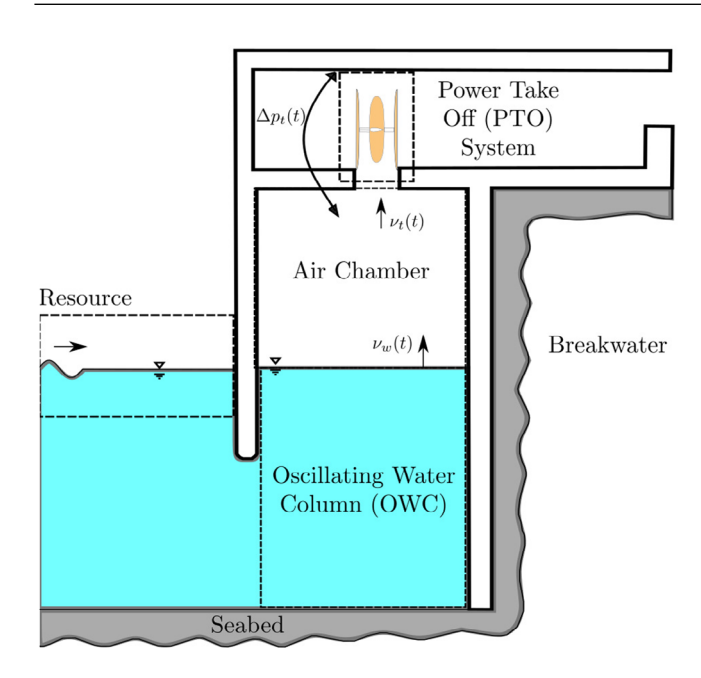


FIGURE 1 OWC system with the chamber fixed to a breakwater.

Therefore, in recent studies, the use of SOSM fixed-gain algorithms to control a variety of OWC-WEC types was successfully explored [30–32], aiming to preserve the attractive robust features, while targeting improved mechanical behaviour of the controlled system. In [30, 31] a control objective which regulates constant speed is proposed whereas, in [32], the authors develop a speed tracking strategy to guarantee operation at the optimal mechanical conversion point.

Despite the improvements achieved with fixed-gain SOSM algorithms, it is acknowledged that there can still be an undesired presence of chattering in certain practical cases. This issue may arise in wide-ranging WEC operating conditions, which only admit to be conservatively bounded, often resulting in the use of excessively large gains [33].

To overcome this limitation, adaptive SOSM techniques have been developed, offering variable-gain SOSM controllers with improved performance. Several design procedures have been proposed in the literature, and these techniques have been successfully applied in various fields [33–37].

In particular, the authors of [38–40] have developed a variable-gain SOSM design technique known as Switched/Time-Based Adaptive (STBA). This method utilizes the finite switching frequency inherent in practical SMC implementations. By counting the zero-crossings of the sliding variable within a specific time window, the STBA method adaptively adjusts the controller gains. It offers several attractive features, including robustness, reduced chattering, relatively low computational cost, and ease of real-time implementation. Additionally, the STBA method has been found to be particularly suitable for controlling wind energy conversion systems [41, 42], which can be considered a related field to OWC control.

Therefore, motivated by its suitability for the control of wind turbines, the STBA approach is used in this paper to develop

a variable-gain SOSM control setup to enhance the power generation efficiency of an on-shore OWC-WEC, composed of a self-rectifying air-driven axial turbine. The control strategy is designed to maximize the power extracted in the power-take-off (PTO) system and is validated by computer simulation of a complete wave-to-wire model.

Thus, the main contribution of this paper is the use of the STBA approach to develop an adaptive-gain SOSM control setup to improve the power generation of an on-shore OWC-WEC, which achieves maximum mechanical power extraction in the OWC-WEC power take off system. In addition, the proposed controller provides smooth control actions, which protect the actuators and consume less energy, and reduce torque oscillations, for lifetime extension of the mechanical rotational parts. Simulation validation is provided by a full waveto-wire model, that is, considering irregular waves, water column hydrodynamics, air compression and generator dynamics. Furthermore, implementation of the control structure utilises a simple and low computational cost control technique which only employs the zero-crossing count of the sliding variable on a time window, showing superior tracking and regulation behaviour when compared against a PID.

2 | MODEL FOR OWC-WEC WITH SYNCHRONOUS GENERATOR

The OWC-WEC system can be schematically divided into three stages [43]. The first stage is the wave capture chamber, which harnesses the energy from the waves to produce an oscillating airflow at its top (see Figure 1). This airflow goes through the PTO system comprising stages 2 and 3. Stage 2 is the self-rectifying turbine, that converts the bidirectional airflow into unidirectional rotational movement, while stage 3 comprises the generator that transforms the shaft mechanical energy into electrical power.

2.1 | Capture chamber

The capture chamber is a semi-submerged fixed structure, the lower part of which is open to the sea water below the still water level, such that the waves produce an oscillating water column inside. This piston-like movement generates a bidirectional airflow at the opening on top of the chamber, where the air turbine is situated. Two models can be used to describe the dynamics inside the capture chamber.

2.1.1 | OWC hydrodynamic model

The movement of the water inside the capture chamber is described [44] by:

$$(m_w + m_\infty)\dot{\nu}_w(t) = -\rho_w g A_c \chi_w(t) - \Delta p_t(t) A_c +$$

$$+ f_e(t, \zeta) - f_r(t, \nu_w), \qquad (1)$$

$$\dot{\chi}_w(t) = \nu_w(t).$$



Here χ_w is the vertical displacement of the free surface of the water, ν_w its speed (see Figure 1) and m_w is the mass of the oscillating water body. g is the gravity constant, ρ_w the water density, and the constant m_∞ the added mass at infinite frequency. The capture chamber area is denoted by \mathcal{A}_c . The pressure oscillation inside the chamber is defined as $\Delta p_t(t) = p_c(t) - p_{\text{atm}}$, where p_c is the pressure oscillation inside the chamber and p_{atm} the atmospheric pressure. Note that the time dependence will be used in the text if a new variable is defined; otherwise, it only will appear in equations when necessary. Then, f_e is the excitation force, dependent on the free water surface elevation, ζ , and f_r is the radiation force, with both forces determined as in [44].

2.1.2 | Air chamber model

The air in the OWC chamber is modelled as an ideal gas, the process of compression/decompression of the air is assumed to be isentropic, and the pressure distribution inside the chamber assumed to be uniform [45]. The equation for the dynamics of the pressure, considering a linear turbine, [46] is:

$$\Delta \dot{p}_t(t) \frac{V_0}{c^2} = \rho_c(t) \nu_w(t) A_c - \frac{K_c 2r}{\Omega_w(t)} \Delta p_t(t). \tag{2}$$

Here Ω_m is the turbine rotational speed, r is the turbine radius, c is the speed of sound in air, V_0 is the chamber volume in unperturbed conditions, and the air chamber density, ρ_c , is:

$$\rho_{\epsilon}(t) = \rho_{\text{atm}} \left(\frac{\Delta p_t(t)}{p_{\text{atm}}} + 1 \right)^{1/\gamma}.$$
 (3)

Finally, K_c is a constant dependent on the turbine geometry, which relates the flow rate with the pressure head in a linear turbine.

2.2 | PTO air turbine

The first part of the PTO is the self-rectifying air turbine, an energy extracting turbomachine that rotates in a single direction, regardless of the bidirectional flow of air. Examples of such turbines include the Wells turbine [47], impulse turbine [48] and bi-radial turbine [49]. The OWC-WEC under study in this paper utilises a Wells device (a linear turbine), which is the most popular OWC turbine, presenting relatively simple operation and reduced cost, with model [47]:

$$\Delta p_{x}(t) = C_{a}(\phi(t))K_{t}\rho_{\text{in}}(t)\frac{1}{A_{t}}\left[\nu_{x}^{2}(t) + \left(r\Omega_{m}(t)\right)^{2}\right], \quad (4)$$

$$\phi(t) = \frac{\nu_{x}(t)}{r\Omega_{m}(t)},\tag{5}$$

$$T_t(t) = C_t(\phi(t))K_t\rho_{\text{in}}(t)r\Big[\nu_x^2(t) + (r\Omega_m(t))^2\Big], \qquad (6)$$

$$\eta(t) = \frac{P_{\text{out}}(t)}{P_{\text{in}}(t)} = \frac{T_t(t)\Omega_m(t)}{\nu_x(t)A_t\Delta p_x(t)},\tag{7}$$

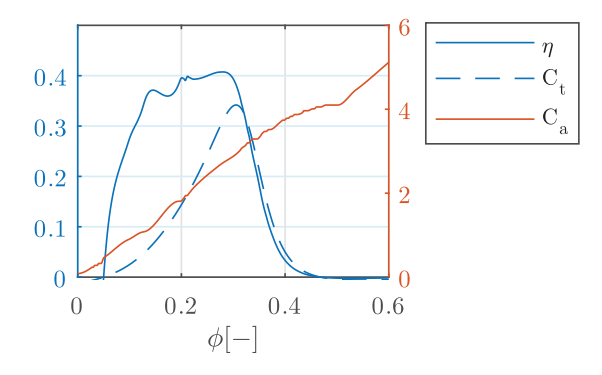


FIGURE 2 Wells turbine coefficients [50]. C_i : Torque coefficient, C_a : pressure coefficient, η : turbine pneumatic efficiency.

where Δp_x and ν_x are the 'rectified', or absolute values, of the pressure drop, and the airflow speed through the turbine, respectively, that is, $\Delta p_x = |\Delta p_t|$ and $\nu_x = |\nu_t|$. ν_t is obtained from the expression of the mass flow rate through the turbine, $\dot{m}_t = \rho_{\rm in} A_t \nu_t$, where $\rho_{\rm in}$ [44] is:

$$\rho_{\text{in}}(t) = \begin{cases} \rho_{c}, & \text{if } \Delta p > 0 \text{ (exhalation),} \\ \rho_{\text{atm}}, & \text{if } \Delta p \leq 0 \text{ (inhalation).} \end{cases}$$

 $C_a(\phi)$ is the pressure coefficient, a nonlinear function of the flux coefficient (ϕ) , defined in (5). Equation (6) relates to the turbine torque (T_t) , with $C_t(\phi)$ the torque coefficient. $K_t = nlb/2$ is the turbine constant, with n, b and l, the number, height and chord length of the blades, respectively, and A_t is the turbine air duct area. Lastly, (7) expresses the turbine pneumatic efficiency, $\eta(\phi)$. The turbine coefficients $C_a(\phi)$, $C_t(\phi)$ and $\eta(\phi)$ illustrated in Figure 2.

2.3 | Permanent magnet synchronous generator

The second part of the PTO is the generator, with different types currently in use in OWC-WECs, for instance, squirrel cage induction generators [44], doubly fed induction generators (DFIG) [32, 51] and synchronous generators [30]. The WEC topology under study, in this work, utilises a permanent magnet synchronous generator (PMSG), taking advantage of its low maintenance, extended speed operational range, good energy efficiency and capability to comply with grid code requirements [52]. It can be modelled [53] as:

$$\begin{bmatrix} \dot{i}_{d} \\ \dot{i}_{q} \\ \dot{\Omega}_{m} \end{bmatrix} = \begin{bmatrix} -\frac{R_{d}}{L_{d}} i_{d}(t) + \frac{L_{q}}{L_{d}} i_{q}(t) p_{p} \Omega_{m}(t) \\ -\frac{R_{q}}{L_{q}} i_{q}(t) - \left(\frac{L_{d} p_{p}}{L_{q}} i_{d}(t) + \frac{\psi_{a} p_{p}}{L_{q}} \right) \Omega_{m}(t) \\ T_{t}(t)/J - T_{e}(t)/J - B_{w} \Omega_{m}(t)/J \end{bmatrix} + \begin{bmatrix} 1/L_{d} & 0 \\ 0 & 1/L_{q} \\ 0 & 0 \end{bmatrix} \begin{bmatrix} v_{d}(t) \\ v_{q}(t) \\ 0 \end{bmatrix},$$
(8)

where ψ_a is the inductive coupling flux, p_p is the number of pole pairs, $R_d = R_q = R_s$ and $L_d = L_q = L_s$ are stator



resistance and inductance, respectively, assuming a uniform air gap flux. v and i represent the direct ($_d$) and quadrature ($_q$) stator voltages and currents, respectively, and J is the lumped inertia of the system moving parts (turbine and generator) and B_w is the viscous friction coefficient. The electromagnetic torque is evaluated as:

$$T_{e}(t) = p_{p}[(L_{d} - L_{q})i_{d}(t) + \psi_{a}]i_{q}(t).$$
 (9)

3 | CONTROL DESIGN FOR THE PMSG BASED OWC-WEC

In this section, an energy-maximising control for the PTO system is designed. While many WEC control strategies focus on maximisation of hydrodynamic (to mechanical) energy conversion [54], the OWC has the particular characteristic that the crucial component is the air turbine, so operating it at an optimal point is crucial to maximising power extraction. Note that the system model in Section 2 contains a full description of the key system components, including the turbine, chamber dynamics (including air compressibility) and generator.

Specifically, focus is on the application of an adaptive second order sliding mode control technique to the OWC PTO system. The algorithm used here is an adaptive twisting controller, first developed in [26, 39, 40]. Based on the robust design framework of the twisting algorithm, the adaptation mechanism reduces the gains when possible, keeping them at the minimum values that guarantee sliding mode operation, and enlarging them only when disturbances increase. In an improbable worst case situation, the algorithm operates as a classical twisting SMC.

Sliding mode control theory is based on the introduction of a 'sliding' function, σ , according to the control objectives. This function is guided to zero by a high-frequency switching control action which is, ideally, infinite in frequency. Then, once $\sigma=0$ is achieved, the control objectives are accomplished [18]. Second order sliding modes inherit SMC advantages such as guiding the system to the sliding surface (for SOSM, $\sigma=\dot{\sigma}=0$) in finite time, and keeping it there robustly despite model uncertainty and perturbations. Then, following [40], the control scheme, when the control actuator has finite bandwidth, is improved via gain adaptation.

The control structure is designed for the PTO model using, as control inputs, the generator voltages v_q and v_d . A scheme of the control structure is shown in Figure 3.

3.1 | Control objectives and sliding variables

Two control objectives are pursued in this work. The first focuses on maximising power production [55], while the second relates to mechanical stress reduction, specifically aiming to minimise electromagnetic torque oscillations.

3.1.1 | Objective 1 - energy maximisation

The proposal to accomplish the first objective is based on forcing the PTO to work at the optimal operation point. In [32], the

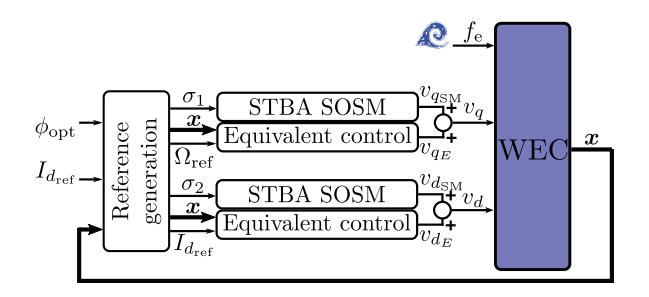


FIGURE 3 Control structure scheme. The states of the system are represented by the vector $\mathbf{x} = \begin{bmatrix} z_w & \nu_w & \Delta p_t & \Omega_m & i_q & i_d \end{bmatrix}^T$. The control references $I_{d_{\text{ref}}}$ and Ω_{ref} , as well as the sliding variables σ_1 and σ_2 (all defined in Section 3.1), are used in the control calculations. The control actions v_q and v_d are determined in Sections 3.2 and 3.3.

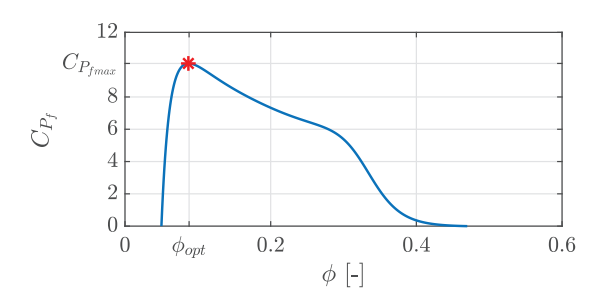


FIGURE 4 Power coefficient, C_{P_f} , has an unique maximum value in $\phi = \phi_{\text{opt}}$.

authors proposed that the turbine mechanical output power can be expressed, from (7) and (4), as:

$$P_{\text{out}} = \underbrace{\frac{2K_f}{A_t} \eta(\phi) C_a(\phi) \left(1 + \phi^{-2}\right)}_{C_{P_f}(\phi)} \underbrace{\frac{\rho_{\text{in}} A_f}{2} \nu_x^3}_{P_f} =$$

$$= C_{P_f}(\phi) P_f(\nu_x, \Delta p_t).$$
(10)

The function $P_f(\nu_x, \Delta p_t)$ depends on the air flux and the pressure drop. The bidirectional air flux, ν_t , is calculated using the continuity equation for compressible fluids as $\nu_t = \rho_c(t) \mathcal{A}_c \nu_w(t) / \rho_{\text{atm}} \mathcal{A}_t$. As a result, $P_f(\nu_w, \Delta p_t)$ is influenced only by these states (see Figure 3). Additionally, the coefficient C_{P_f} is determined by the operating point, given by the flow coefficient ϕ . It exhibits a unique maximum (see Figure 4) obtained from the coefficients in Figure 2, which allows for the identification of an optimal operational condition. It is worth noting that the efficiency curve in Figure 4 encompasses all chamber/turbine characteristics.

The objective, to keep the system working at its optimal point, $\phi = \phi_{\rm opt}$, can be achieved by tracking the optimal rotational speed:

$$\Omega_{\rm opt}(t) = \frac{\nu_x(t)}{r\phi_{\rm opt}}.$$
 (11)

Establishing a speed setpoint for the turbine has become an established practice for OWC control [7], and reflects the



dominant characteristics of the turbine (indicated by the sharp peak in C_{P_f}) in the power train. In order to avoid the relatively poor starting characteristics of the Wells turbine, a minimum rotational speed value was defined following exhaustive analysis, considering the trade-off between turbine depowering and optimum operation. Consequently, the rotational speed reference is defined as:

$$\Omega_{\text{ref}}(t) = \begin{cases} \Omega_{\text{opt}}(t) & \text{if } \Omega_{m}(t) \ge \Omega_{\text{min}}, \\ \Omega_{\text{min}} & \text{if } \Omega_{m}(t) < \Omega_{\text{min}}, \end{cases}$$
(12)

with a corresponding sliding variable:

$$\sigma_1(t) = \Omega_m(t) - \Omega_{\text{ref}}(t). \tag{13}$$

3.1.2 | Objective 2 - mechanical stress reduction

It has been shown that oscillations in the electromagnetic torque are heavily attenuated when i_d is forced to zero [56]. Hence, to reduce the mechanical fatigue in the turbine and, consequently, extend its lifetime, the second objective prompts the following condition:

$$I_{d_{rat}} = 0. (14)$$

The condition in (3.1.2), in turn, suggests a choice of the second sliding variable as:

$$\sigma_2(t) = i_d(t) - I_{d_{ref}} = i_d(t).$$
 (15)

3.2 | Framework for the adaptive gain control design

As previously explained, the controllers for the OWC-WEC in this work are based on a twisting algorithm, with a gain adaptation feature. A necessary first step in the control design procedure involves the development, and tuning, of a standard fixed-gain twisting controller, which serves as framework for the final controller.

Important remarks: The sliding variables defined in (13) and (15) are input-output decoupled with respect to v_q and v_d , respectively; thus, it is possible to design two independent single-input single-output control schemes, instead of realising a MIMO design. In addition, it can be easily determined that $\sigma_1(\sigma_2)$ is of relative degree 2(1) with respect to $v_q(v_d)$.

The control scheme proposed here comprises two terms, one for each control input:

$$v_i = v_{i_{\rm E}} + v_{i_{\rm SM}},\tag{16}$$

where sub-index i (i = 1, 2) indicates the corresponding objective to be achieved, that is, sliding variables of Sections 3.1.1 and 3.1.2, respectively, with $v_1 = v_q$ and $v_2 = v_d$.

The first term, $v_{i_{\rm E}}$, involves a continuous action which provides the bulk of the control effort, supplemented by smaller gains for SOSM action embedded in the second control term.

To obtain $v_{i_{\rm E}}$, a procedure inspired by the concept of equivalent control in sliding mode [57] is followed.

On the other hand, $v_{i_{\rm SM}}$ is a SOSM term based on the twisting algorithm. This term guarantees:

- Robustness with respect to various internal and external bounded disturbances and to unmodelled dynamics.
- Accurately regulating and tracking different kind of variables, with finite-time convergence.
- Reduction of mechanical stresses and chattering (i.e. highfrequency vibrations of the controlled system), compared to standard SM strategies, given that the applied control actions are continuous.
- Simple control laws, easy to implement, which can be designed based on nonlinear models.

3.2.1 | First control term, v_{i_E} , design

Here, the procedure followed for obtaining the continuous control actions, $v_{q_{\rm E}}$ and $v_{d_{\rm E}}$, for the two control objectives identified in Sections 3.1.1 and 3.1.2, is shown.

First of all, the sliding variable associated with the first control objective, σ_1 , has relative degree (RD) 2. So, for the determination of v_{q_E} , a control expression affine in the second derivative of σ_1 is needed (the control action v_q appears explicitly there).

$$\ddot{\sigma}_{1} = \frac{1}{J}\dot{T}_{t} + \frac{K_{g}}{J}\left(-\frac{R_{s}}{L_{s}}i_{q} - i_{d}p_{p}\Omega_{m} - \psi_{a}p_{p}\Omega_{m}/L_{s}\right) - \frac{B}{J}\dot{\Omega}_{m} - \ddot{\Omega}_{ref} + \frac{K_{g}}{JL_{s}}v_{q} = a_{1}(x, t) + b_{1}(x, t)v_{q},$$

$$(17)$$

where $K_g = p_p \psi_a$ is the generator constant and $T_t(\nu_x, \Omega_m)$ can be obtained by differentiating (6) with respect to time. ν_{q_E} is the continuous control action which maintains $\sigma_1 = \dot{\sigma}_1 = 0$ in nominal conditions, assuming no perturbations or uncertainty:

$$v_{q_{\rm E}} = v_q \Big|_{\sigma_1 = \dot{\sigma}_1 = \ddot{\sigma}_1 = 0} = -\frac{a_{1_{\rm NOM}}(x, t)}{b_{1_{\rm NOM}}(x, t)} \Big|_{\sigma_1 = \dot{\sigma}_1 = \ddot{\sigma}_1 = 0}.$$
 (18)

Second, to obtain the continuous control v_{d_E} for the second control objective, the procedure is similar to the previous one. It starts by determining the first derivative of σ_2 , where v_d appears explicitly:

$$\dot{\sigma}_{2} = \dot{i}_{d} - \dot{I}_{d_{\text{ref}}} = -\frac{R_{s}}{L_{s}} i_{d} + i_{q} p_{p} \Omega_{m} + \frac{1}{L_{s}} v_{d}$$

$$= A_{2}(x, t) + B_{2}(x, t) v_{d}.$$
(19)

Then, isolating v_d from (19) and evaluating in nominal conditions, when $\sigma_2 = 0$, the expression to compute $v_{d_{\rm E}}$ can be derived as:

$$v_{d_{\rm E}} = v_d \Big|_{\sigma_2 = \dot{\sigma}_2 = 0} = -\frac{A_{\rm 2_{NOM}}(x, t)}{B_{\rm 2_{NOM}}(x, t)} \Big|_{\sigma_2 = \dot{\sigma}_2 = 0}.$$
 (20)



3.2.2 | Second control term, v_{ism} , design

The twisting controller algorithm [26] with fixed gains, has the following expression:

$$v_{i_{\text{SM}}}(\sigma_i) = -r_i \operatorname{sign}(\sigma_i) - r_i' \operatorname{sign}(\dot{\sigma}_i); \ r_i > r_i' > 0.$$
 (21)

The general procedure to calculate the gains in (21) involves writing the second derivative of the sliding variable in a control form affine in $v_{i_{\text{SM}}}$:

$$\ddot{\sigma}_{i} = \underbrace{a_{i}(x,t) + b_{i}(x,t)v_{i_{\mathrm{E}}}}_{\lambda_{i}} + \underbrace{b_{i}(x,t)}_{\gamma_{i}}v_{i_{\mathrm{SM}}}.$$
 (22)

Then, the functions λ_i and γ_i must be bounded by three positive constants $\Gamma_{m_i} < \Gamma_{M_i}$ and C_i , as

$$\begin{aligned} |\lambda_i(x,t)| &\leq C_i \\ \Gamma_{m_i} &\leq \gamma_i(x,t) \leq \Gamma_{M_i}. \end{aligned} \tag{23}$$

This is a key part of the SOSM control design, as it provides robustness in all the conditions considered when determining the bounds. Once the bounds are established, the fixed gains of the twisting controller are determined as:

$$r_{i} = r'_{i} + \Delta_{T_{i}}$$

$$r'_{i} > \frac{\Delta_{T_{i}}(\Gamma_{M_{i}} - \Gamma_{m_{i}}) + 2C_{i}}{2\Gamma_{m_{i}}}$$

$$\Delta_{T_{i}} > \frac{C_{i}}{\Gamma_{m_{i}}}.$$
(24)

Satisfaction of the conditions in (24) guarantees finite time convergence and robust maintenance of the system states on $\sigma_i = \dot{\sigma}_i = 0$ as has been proven in [25]. In the following, the method of application for each sliding variable is shown.

For σ_1 , (17) is rearranged to the form of (22) to obtain λ_1 and γ_1 , completing the gain calculations for the twisting term ν_{act} :

$$\ddot{\sigma}_{1} = \underbrace{a_{1}(x,t) + \frac{K_{g}}{JL_{s}} v_{q_{E}}}_{\lambda_{1}(x,t)} + \underbrace{\frac{K_{g}}{JL_{s}}}_{\gamma_{1}(x,t)} v_{q_{\text{SM}}}.$$
(25)

Alternatively, the sliding mode term calculation process for σ_2 starts by expanding the system and defining the control variable $\nu_I = \dot{\nu}_{d_{SM}}$, so σ_2 is of RD = 2 with respect to ν_I .

Then, to obtain the bounds for the gains of the twisting term, the second time derivative of σ_2 is calculated:

$$\ddot{\sigma}_{2} = \underbrace{-\frac{R_{s}}{L_{s}}\dot{i_{d}} + \dot{i_{q}}p_{p}\Omega_{m} + i_{q}p_{p}\dot{\Omega}_{m} + \frac{\dot{\nu}_{d_{E}}}{L}}_{\lambda_{2}(x,u,t)} + \underbrace{\frac{1}{L_{s}}}_{\gamma_{2}(x,t)}\nu_{I}. \tag{26}$$

The gain calculation process ends when the functions λ_i and γ_i (i = 1, 2) are bounded as in (23), and the bounds are then utilised to calculate the gains following (24).

Finally, note that the closed loop system trajectories are completely determined by the proposed controller, guaranteeing the system stability. Specifically, the design model in (8) has three states, with a further state added for the implementation of twisting in (21). Also, the SOSM control structure ensures that the following conditions $\sigma_1 = \dot{\sigma}_1 = \sigma_2 = \dot{\sigma}_2 = 0$ are achieved.

3.3 | Adaptive gain design

In this section, the adaptation mechanism of the variable-gain Twisting controller is presented and designed for the OWC-WEC. The objective is to minimise the discontinuous control effort while ensuring operation in a predefined 'real sliding mode operation' criterion. The design of this mechanism relies on prior knowledge of the system, taking into account the finite time frequency switching (f_c) associated with the practical actuator and the appropriate selection of gain values.

The adaptation policy is based on counting the zero crossings of the sliding variable, $N_{\rm sw}$, during appropriate time windows of length T_v . Then, the occurrence of a real sliding mode is verified by checking whether such a count value is large enough, in accordance with a predefined sliding mode existence criterion, $N_{\rm sw} \geq N$. Subsequently, if the number of crossings counted in the window is greater than the threshold, the algorithm detects that the system is operating in a real sliding mode and decreases the gains by $-\Lambda T_v$ (Λ is called decrement slope). On the other hand, if the crossing count is lower than the threshold, it means that the system is escaping more than desired from the surface, so the gains are increased by $+\Lambda' T_v$ (Λ' : increment slope) to return quickly to the sliding surface. The slopes for the controller are designed [40] as:

$$\Lambda_{i} > 0$$

$$\Lambda'_{i} > \Lambda_{i} + 2|\dot{\lambda}_{i}|/\Gamma_{m_{i}},$$
(27)

where λ_i and Γ_i (i = 1, 2) are the same functions and bounds, respectively, calculated for each objective in Section 3.2. The verification of (27) guarantees that the system will return in a short time to the sliding surface. To compute the increment slope, it is necessary to differentiate the λ_i functions corresponding to each sliding variable.

The adaptive twisting control algorithm has the form:

$$v_{(q \text{ ord})_{\text{SM}}}(\sigma_i) = -\alpha_{T_i} W_i^j \operatorname{sign}(\sigma_i) - W_i^j \operatorname{sign}(\dot{\sigma}_i), \qquad (28)$$

where the *i* subscript indicates the controller for Objectives 1 and 2, respectively, $\alpha_{T_i} = r_i/r'_i$ (with r_i and r'_i defined in (23)), and W_i^j is the variable gain, which is updated according to [39]:

$$\begin{aligned} W_{i}^{1} &= W_{\max_{i}} = r_{i}', \\ W_{i}^{j+1} &= \begin{cases} \max(W_{i}^{j} - \Lambda_{i} T_{v}, W_{\min_{i}}) & \text{if } N_{\text{sw}}^{j} \geq N \\ \min(W_{i}^{j} + \Lambda_{i}' T_{v}, W_{\max_{i}}) & \text{if } N_{\text{sw}}^{j} < N \end{cases}, \end{aligned}$$
(29)



where the superscript index j indicates the time window interval $(jT_v; (j+1)T_v]$, $W_{\max_1} = r_1'$ and $W_{\max_2} = r_2'$. Also, W_{\min_j} is the minimal positive value that the algorithm could select, and is arbitrarily defined. Then, the window length T_v (the same for both controllers) is defined as a multiple integer of the commutation period $T_c = 1/f_c$, large enough to capture a sufficient amount of potential crossings, but sufficiently small so as to react sufficiently quickly. Finally, the threshold N is determined by observation of the zero crossings of the sliding variable, for each objective [40].

This results in an adaptive controller with the ability to adjust the control gains online, keeping the control magnitude at a minimum admissible level.

4 | SIMULATION RESULTS

This section is divided into four subsections that focus on specific results. First, Section 4.1 presents the gain calculation procedure for the design model, which only considers the PTO dynamics. Then, Section 4.2 analyzes the behavior and advantages of the designed adaptive SOSM control, specifically regarding the control inputs and outputs. In Section 4.3, a comparison is made between the performance of a PID controller, the twisting controller with fixed gains, and the twisting controller with adaptive gains, all with the v_{i_E} term added. Finally, Section 4.4 contrasts the energy extracted with the different control strategies simulated in the full wave-to-wire model of Section 2, which considers the dynamics of water movement, air compression, and the electrical system. Note that only Section 4.1 uses the design model for simulations, while the other sections use the full model. The simulations are based on the wave climate of Mar del Plata, Buenos Aires, Argentina, with varying parameters of wave height, $H_{\rm s}$, and wave peak period, T_b , as shown in the scatter plot in

4.1 | Gain determination

The SOSM design process is summarized as follows. To determine the fixed gains of the SOSM controller, bounds covering all possible inputs, uncertainties, and perturbations are computed. Exhaustive simulations are run with different sea states, electrical parameter uncertainties of 15%, and torque perturbations up to 10% of turbine torque T_t . The system is also exposed to different realizations of the excitation input within a range of $0.5 \le H_s \le 2 \text{m}$ and $6 \le T_p \le 12 \text{s}$ to cover the most probable wave climate region (see Figure 5). Figure 6 shows a sample of the results, where the bounds are designated as C_i with a red dashed line. The gains for the twisting controller are then calculated using these bounds (Table 1).

The design process also considers the frequency limitation of the actuators, modeled with the commutation frequency of 2 kHz. For the STBA SOSM controller, a threshold of N=3 is determined, and a window of $T_v=15$ ms is selected to capture sufficient sliding variable crossings. The minimum gain values

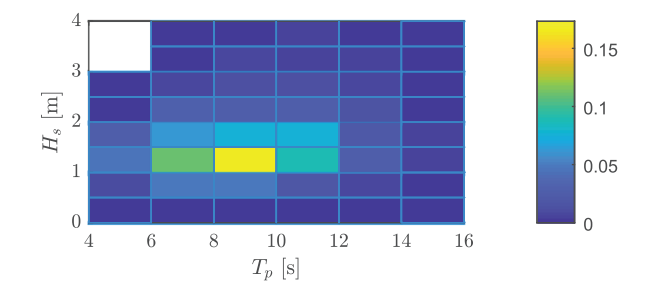


FIGURE 5 Mar del Plata's wave climate probability chart.

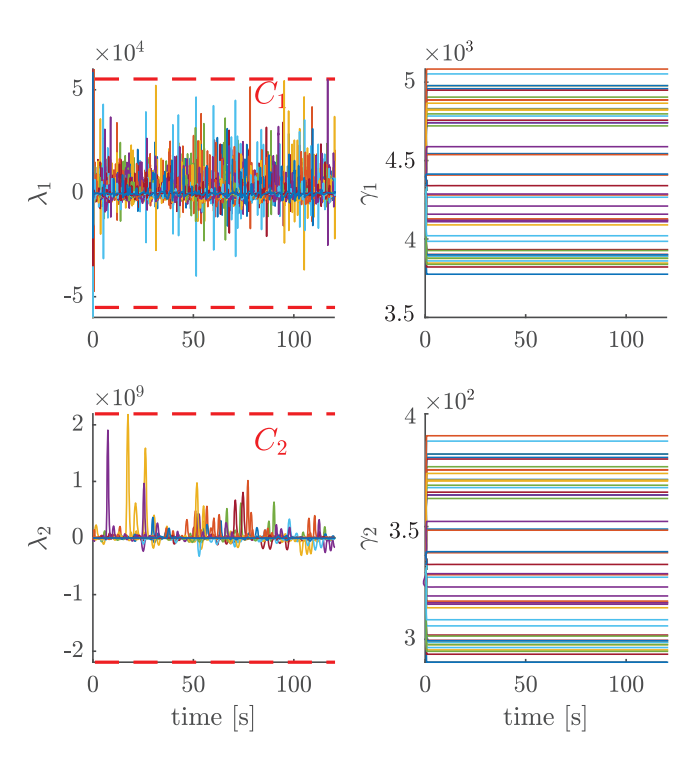


FIGURE 6 Bound calculations, after several simulations, for σ_1 (1st row) and σ_2 (2nd row). $\lambda_{1,2}$ contains the variation of the system for different wave climates, perturbation and uncertainty. $\gamma_{1,2}$ are the probable values in a 15% variation of the electrical parameters with an uniform distribution. Bounds obtained here correspond to a differential inclusion of (25) and (26), respectively.

TABLE 1 System parameters.

Capture chamber	PTO	STBA-SOSM
$A_c = 19.35 \text{ [m}^2\text{]}$	$K_t = 0.1031$	$r_1 = 524$
r = 0.375 [m]	$R_s = 0.08 [\Omega]$	$r_1' = 185$
$A_t = 0.4418 \text{ [m}^2\text{]}$	$L_s = 3 \text{ [mHy]}$	$r_2 = 732.5$
$p_{\text{atm}} = 101325 \text{ [Pa]}$	$\psi_a = 0.31 \text{ [V s]}$	$r_2' = 393.6$
$\rho_{\rm atm} = 1.19 [\rm kg/m^3]$	$p_p = 1$	$\Lambda_1 = 1$
$V_0 = 104.62 [\text{m}^3]$	$J = 0.49 [\text{kg m}^2]$	$\Lambda_1' = 27$
	$B_w = 0.03 [\text{N ms}]$	$N_1 = N_2 = 3$
		$\Lambda_2 = 50$
		$\Lambda'_2 = 728$



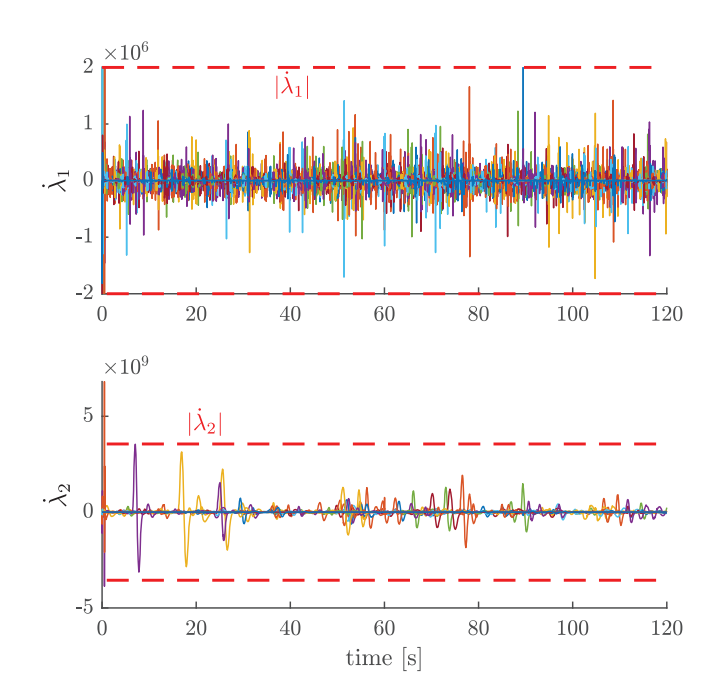


FIGURE 7 Bound computations (red dashed lines) for the increment slope, Λ'_i , calculated for each controller.

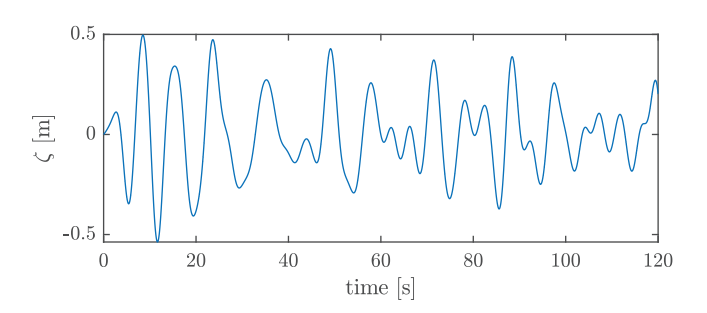


FIGURE 8 Realisation for the free water surface elevation with $H_s = 1m$ and $T_b = 10$ s.

are $W_{\text{min}1} = 1.8$ and $W_{\text{min}2} = 4$, and the increment slope Λ' is calculated using the bounds (Figure 7) and (27). Table 1 summarizes the parameters for the capture chamber, PTO, and STBA SOSM controller.

4.2 | Analysis of controller behaviour

The control design is validated by running several simulations on the wave-to-wire model. Nevertheless, in this subsection and the following, only one example is shown using a typical outcome. The input to the system is the wave of Figure 8 in a 120 s realisation, associated with a JONSWAP wave spectrum with $H_s = 1m$ and $T_p = 10s$ (the most probable wave climate in the area under study).

In Figure 9, the first row shows the control behavior in response to the wave input. The red lines represent the varying control actions, v_q and v_d , which adjust to the input changes. The STBA SOSM controller (in red) requires greater control effort than the $v_{i_{\rm E}}$ controllers (in black) to keep the system on the sur-

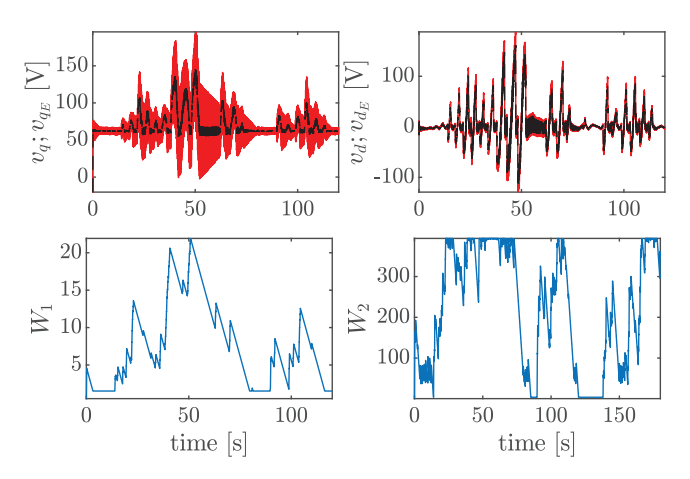


FIGURE 9 Main outcomes of the controller behavioural analysis. In the first row, the control actions are in red, with the equivalent control actions in black. The second shows the variable gain values.

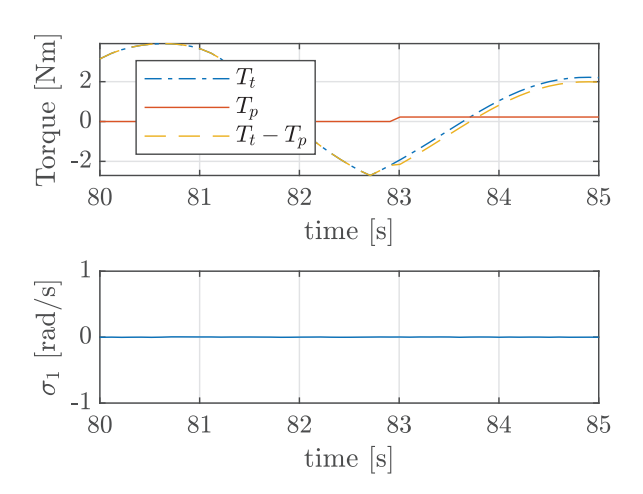


FIGURE 10 Example of control structure robustness. In the upper plot, T_t is the turbine torque, T_p is the perturbation torque and $T_t - T_p$ is the difference between turbine torque and the perturbation. In the lower plot, the evolution of the sliding variable σ_1 shows no changes in its amplitude.

face, providing robustness against uncertainty and disturbances. Furthermore, the second row of Figure 9 displays the evolution in the controller gains, varying in accordance with the STBA SOSM adaptation law.

Furthermore, to showcase the robustness of the proposed control structure, a perturbation equivalent to 10% of the turbine torque, T_t , caused by an increase in viscous friction of the generator (i.e. Equation (8), $T_p = \Delta B_w * \Omega_m$) is considered during the simulation at t = 83 s. The occurrence of this perturbation is illustrated in the upper plot of Figure 10. However, in the lower plot of Figure 10, no change is observed in the sliding variable σ_1 , indicating that the control strategy effectively rejects the perturbation considered.

4.3 | Comparison against fixed-gain SOSM and PID controllers

To compare the performance of the designed STBA SOSM controller and the classical SOSM one, simulation results with



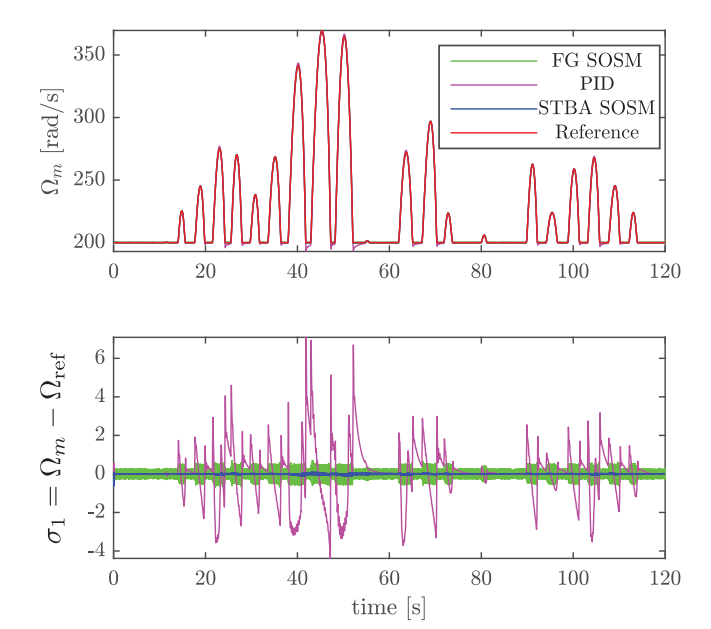


FIGURE 11 Tracking of the sub-optimal speed setpoint of Section 3.1.1 (in red), for the different controllers. The fixed gain SOSM controller is in green, while the PID controller result is in magenta. The blue trace corresponds to the system controlled with the STBA SOSM controller. The upper plot shows the rotational speed of the turbine, while the lower plot shows the error in tracking the speed reference.

the most ubiquitous control scheme, namely a Proportional-Integral-Derivative (PID) controller, are presented. The PID and PI controllers used here are initially tuned using Ziegler–Nichols methods and, then, they are further adjusted through extensive simulation trials. Such tuning looks for a balance in the trade off between fast response time and low overshoot. The final parameters in use are P = 2.94; I = 0.88; D = 0.014 for the rotational speed controller and P = 0.12; I = 62 for the current controller. Those controllers are added to the same control terms of Section 3.2.1 (v_{iv}).

In Figure 11, a comparison of different control strategies for tracking the sub-optimal reference of (12) is shown. The top part of Figure 11 depicts the performance of the various controllers in terms of their ability to track the reference. The Ω_{\min} value used in this study was obtained through empirical analysis of comprehensive simulation tests. The value was selected to achieve maximum energy generation for the given wave climate. As can be observed from the bottom panel of Figure 11, which compares the tracking errors for the different controllers, the PID controller tracking performance is found to be relatively poor, with speed errors up to 7 rad/s, the fixed-gain SOSM controller limits errors to less than 1 rad/s, while the errors are a further order of magnitude lower for the proposed adaptivegain SOSM controller. Furthermore, Figure 11 highlights the benefits of an adaptive SOSM algorithm over the more traditional SOSM fixed-gain controller, which struggles to maintain low chattering operation.

These results emphasize the importance of designing control strategies that can adapt to changing operational conditions, of particular importance in the wave energy application, where a

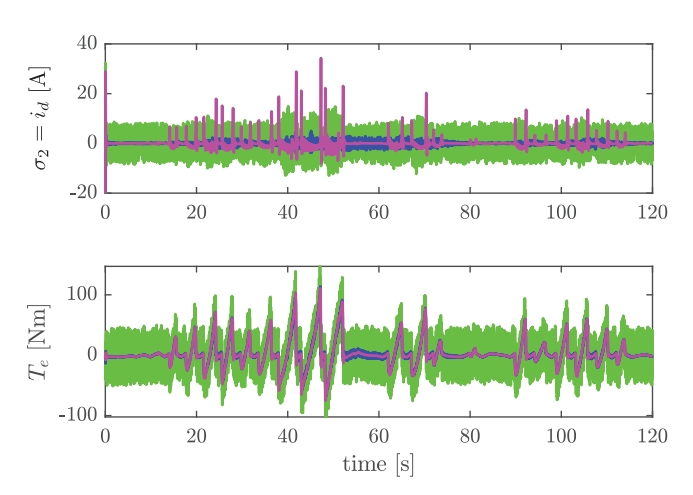


FIGURE 12 Figure on top shows the direct current, i_d , obtained with different controllers, FG SOSM in green, STBA SOSM in blue, and PI in magenta. The reference is $i_d = 0$. The figure on the bottom is the electromechanical torque, T_e , generated by each controller.

wide variety of sea conditions can be experienced at any particular site. The STBA SOSM control strategy presented in this study provides a promising solution to this challenge, demonstrating its ability to outperform a traditional PID controller in tracking the turbine velocity reference, and substantially reduces output chattering compared with fixed gain SOSM schemes.

Figure 12 illustrates the results obtained for the second control objective, which is to reduce torque oscillations in the system. The top plot of Figure 12 shows the evolution of i_d for the different controllers employed, where the performance of the STBA SOSM approach stands out due to its very tight regulation performance. It is noteworthy that the STBA SOSM controller displays significantly lower chattering than the fixedgain SOSM design, while also being more robust than the PI controller, with robustness articulating the capacity to keep tight regulation of the variable despite uncertainty and perturbation. The bottom plot in Figure 12 depicts the electromagnetic torque, T_e , for the different control strategies, clearly showing the significant reduction of the torque oscillations when the fixed-gain SOSM controller is replaced by the STBA SOSM controller. This is an important improvement, as torque oscillations in WEC systems can cause structural damage and decrease the overall efficiency of the energy conversion process.

The improved performance of the proposed STBA SOSM, regarding chattering, can be noticed by observation of Figure 11 (where the lower plot corresponds to the error in speed, i.e. σ_1) and Figure 12 (where the upper plot, current i_d , coincides with σ_2). A significant chattering reduction is observed in both sliding variables when the STBA SOSM is compared against the fixed gain SOSM controller. To allow for a quantitative measure of the improvement, the standard deviation (std) has been calculated for both sliding controllers and the PI/PID controllers. The results are in Table 2, where a reduction of 7 to 10 times, with respect to the fixed gain controller, is obtained with the STBA SOSM. Most of this std reduction is due to the gain adaptation proposed, which reduces the chattering in the outputs and, consequently, the deviation of the sliding



TABLE 2 Standard deviation calculated for the sliding variables.

	Fixed gains	STBA	PID/PI
std σ_1	0.2	0.02	1.2
std σ_2	17.9	2.5	3.95

TABLE 3 Electrical energy extracted with the different control strategies after 1h (measured in Wh).

	Fixed gains	STBA	PID
SS1	2.70E+05	6.25E+05	5.91E+05
SS2	4.33E+06	4.68E+06	4.39E+06
SS3	2.84E+06	3.20E+06	2.78E+06
SS4	2.17E+07	2.19E+07	2.15E+07

variable from $\sigma = 0$. On the other hand, the STBA SOSM also has a significantly lower std, compared to the linear PI/PID controller, thanks to the robustness against system uncertainty and perturbations provided by STBA SOSM controller.

4.4 | Generated energy analysis

Finally, a comparison of the energy extracted by the control strategies described in the previous section is made. In order to evaluate the strategies in different conditions, four sea states are simulated:

- **SS1**: $H_s = 0.5m$; $T_p = 10$ s,
- SS2: $H_s = 1m$; $T_b = 10 \text{ s}$,
- **SS3**: $H_s = 1.5m$; $T_b = 8$ s,
- **SS4**: $H_s = 2m$; $\dot{T}_b = 12 \text{ s.}$

The simulations run up to 1b (of simulation time), and the results of the energy extracted in that period are shown in Table 3.

Note that, for less energetic sea states, such as SS1, the difference between the fixed gain and STBA SOSM is significant, since considerable energy is lost due to chattering in the fixed-gain case. Also, it is interesting to observe that, when the sea state has a relatively short predominant period, the sliding mode techniques perform better than the PID controller, which can be explained by the limited accuracy of the PID strategy at following the reference. Finally, when the sea state is very energetic, and with a long predominant period, the differences between the control strategies are reduced. However, in all the cases observed, the STBA SOSM approach obtains more energy (Table 4).

5 | CONCLUSIONS

This paper develops a robust control strategy for an oscillating water column system with a Wells turbine and a permanent magnet synchronous generator. By using an adaptive second order

TABLE 4 Difference of energy obtained with the STBA SOSM approach against the other strategies.

STBA vs.	Fixed gains	PID
SS1	131.48%	5.75%
SS2	8.08%	6.60%
SS3	12.67%	15.10%
SS4	0.92%	1.86%

sliding mode control technique, the system can achieve two control objectives: tracking the optimal turbine rotational speed to extract maximum mechanical power and regulating the direct current of the generator to reduce torque oscillations.

The use of switched time based adaptive second order sliding mode controller is a crucial aspect of this approach, as it deals with the realistic response time of the actuator. The fixed gains second order sliding mode controller often leads to chattering, which is unacceptable in practical applications. The comparison with the classic PID control scheme highlights the superior performance of the adaptive second order sliding mode control technique. A possible alternative to adaptive SOSM, which also reduces chattering, is fuzzy fractional-order SMC [58], but this is beyond the scope of the current study.

Another advantage of the proposed control strategy is its robustness to uncertainties in electrical parameters, torque perturbations, and unmodelled dynamics in the control design. This robustness ensures that the control strategy is practical and reliable in real-world scenarios. For example, the control strategy can account for the air compressibility and hydrodynamics of the capture chamber in the oscillating water column model.

The comparison of the switched time based adaptive second order sliding mode approach with the fixed gain controller and the PID further emphasizes the benefits of the proposed control strategy. The control strategy proposed in this paper extracts significantly more energy than the other two controllers, demonstrating its potential to improve the efficiency of the oscillating water column system.

In conclusion, this paper presents a promising approach to control the oscillating water column system for efficient energy extraction. The use of an adaptive second order sliding mode controller, combined with robustness to uncertainties and superior performance compared to traditional control schemes, makes this approach a valuable contribution to the field of wave energy extraction. However, some challenges still need to be addressed, such as the persistence of a small level of chattering. While the level of chattering is small, and will cause no concern for many of the variables concerned (e.g. the turbine velocity signal has a significant amount of associated mechanical inertia, while the i_d is a purely electrical quantity), further refinement may improve the controller effectiveness, for example in reducing electrical losses, and further research is recommended.

AUTHOR CONTRIBUTIONS

Facundo D. Mosquera: Data curation; formal analysis; investigation; software; visualization; writing—original draft.



Carolina A. Evangelista: Formal analysis; methodology; supervision; writing—original draft. Paul F. Puleston: Conceptualization; formal analysis; funding acquisition; project administration; resources; supervision; writing—review and editing. John V. Ringwood: Conceptualization; project administration; supervision; writing—review and editing.

ACKNOWLEDGEMENTS

This research was supported by the Facultad de Ingeniería, Universidad Nacional de La Plata (UNLP), CONICET and Agencia I+D+i, from Argentina. John V. Ringwood is supported by Science Foundation Ireland through the (MaREI) SFI Centre for Energy, Climate and Marine, under Grant 12/RC/2302_P2.

CONFLICT OF INTEREST STATEMENT

The authors declare no conflicts of interest.

DATA AVAILABILITY STATEMENT

The data that support the findings of this study are available from the corresponding author upon reasonable request.

ORCID

John V. Ringwood https://orcid.org/0000-0003-0395-7943

REFERENCES

- Wang, L., Isberg, J., Tedeschi, E.: Review of control strategies for wave energy conversion systems and their validation: the wave-to-wire approach. Renewable Sustainable Energy Rev. 81, 366–379 (2018)
- Guo, B., Ringwood, J.V.: A review of wave energy technology from a research and commercial perspective. IET Renew. Power Gener. 15(14), 3065–3090 (2021)
- Mork, G., Barstow, S., Kabuth, A., Pontes, M.T.: Assessing the global wave energy potential. In: International Conference on Offshore Mechanics and Arctic Engineering, vol. 49118, pp. 447

 –454. American Society of Mechanical Engineers, New York (2010)
- Falcão, A.F., Henriques, J.C.: Oscillating-water-column wave energy converters and air turbines: A review. Renew. Energy 85, 1391–1424 (2016)
- Rosati, M., Henriques, J., Ringwood, J.: Oscillating-water-column wave energy converters: A critical review of numerical modelling and control. Energy Convers. Manage. X 16, 100322 (2022)
- Ringwood, J.V.: Wave energy control: status and perspectives 2020. IFAC-PapersOnLine 53(2), 12271–12282 (2020)
- Rosati, M., Ringwood, J., Henriques, J.: A comprehensive wave-to-wire control formulation for oscillating water column wave energy converters. In: Trends in Renewable Energies Offshore, pp. 329–337. CRC Press, Cambridge, MA (2022)
- Ceballos, S., Rea, J., Lopez, I., Pou, J., Robles, E., Osullivan, D.L.: Efficiency optimization in low inertia wells turbine-oscillating water column devices. IEEE Trans. Energy Convers. 28(3), 553–564 (2013)
- Justino, P.A.P., de O Falcão, A.F.: Rotational Speed Control of an OWC Wave Power Plant. J. Offshore Mech. Arct. Eng. 121(2), 65–70 (1999)
- Amundarain, M., Alberdi, M., Garrido, A.J., Garrido, I.: Modeling and simulation of wave energy generation plants: Output power control. IEEE Trans. Ind. Electron. 58(1), 105–117 (2011)
- Mishra, S., Purwar, S., Kishor, N.: Maximizing output power in oscillating water column wave power plants: An optimization based MPPT algorithm. Technologies 6(1), 15 (2018)
- Barambones, O., Cortajarena, J.A., Gonzalez de Durana, J.M., Alkorta, P.:
 A real time sliding mode control for a wave energy converter based on a wells turbine. Ocean Eng. 163, 275–287 (2018)

- Barambones, O., Gonzalez de Durana, J., Calvo, I.: Adaptive sliding mode control for a double fed induction generator used in an oscillating water column system. Energies 11(11), 1–27 (2018)
- Garrido, A.J., Garrido, I., Amundarain, M., Alberdi, M., de la Sen, M.: Sliding-mode control of wave power generation plants. IEEE Trans. Ind. Appl. 48(6), 2372–2381 (2012)
- Utkin, V.I.: Sliding Modes in Control and Optimization. Springer-Verlag, Berlin, Germany (1992)
- Li, S., Yu, X., Fridman, L., Man, Z., Wang, X. (eds.): Advances in Variable Structure Systems and Sliding Mode Control–Theory and Applications. In: Studies in Systems, Decision and Control, vol. 115. Springer International Publishing, Cham (2018)
- Fridman, L., Moreno, J., Iriarte, R. (eds.): Sliding Modes after the First Decade of the 21st Century. In: Lecture Notes in Control and Information Sciences, vol. 412. Springer, Berlin, Heidelberg (2012)
- Shtessel, Y., Edwards, C., Fridman, L., Levant, A.: Sliding Mode Control and Observation. Springer, New York (2013)
- Slotine, J.J., Sastry, S.S.: Tracking control of non-linear systems using sliding surfaces, with application to robot manipulators. Int. J. Control 38(2), 465– 492 (1983)
- Burton, J., Zinober, A.S.: Continuous approximation of variable structure control. Int. J. Syst. Sci. 17(6), 875–885 (1986)
- Kwatny, H.G., Young, K.K.D.: The variable structure servomechanism. Syst. Control Lett. 1(3), 184–191 (1981)
- Young, K.D., Utkin, V.I., Ozguner, U.: A control engineer's guide to sliding mode control. IEEE Trans. Control Syst. Technol. 7(3), 328–342 (1999)
- Martins, N.A., Bertol, D.W.: Robust control: First-order sliding mode control techniques. In: Wheeled Mobile Robot Control, pp. 57–88. Springer, Cham (2022)
- Xiong, X., Chen, H., Lou, Y., Liu, Z., Kamal, S., Yamamoto, M.: Implicit discrete-time adaptive first-order sliding mode control with predefined convergence time. IEEE Trans. Circuits Syst. Express Briefs 68(12), 3562–3566 (2021)
- Levant, A.: Sliding order and sliding accuracy in sliding mode control. Int. J. Control 58(6), 1247–1263 (1993)
- Bartolini, G., Ferrara, A., Levant, A., Usai, E.: On second order sliding mode controllers. In: Young, K., Özgüner, U. (eds.) Variable Structure Systems, Sliding Mode and Nonlinear Control, pp. 329–350. Springer, London (1999)
- Steinberger, M., Horn, M., Fridman, L.: Variable-Structure Systems and Sliding-Mode Control. Springer, London (2020)
- Fridman, L., Moreno, J.A., Bandyopadhyay, B., Kamal, S., Chalanga, A.: Continuous nested algorithms: The fifth generation of sliding mode controllers. In: Recent Advances in Sliding Modes: From Control to Intelligent Mechatronics, pp. 5–35. Springer, Cham (2015)
- Kamal, S., Moreno, J.A., Chalanga, A., Bandyopadhyay, B., Fridman, L.M.: Continuous terminal sliding-mode controller. Automatica 69, 308–314 (2016)
- Suchithra, R., Ezhilsabareesh, K., Samad, A.: Optimization based higher order sliding mode controller for efficiency improvement of a wave energy converter. Energy 187, 116111 (2019)
- 31. Gaebele, D.T., Magaña, M.E., Brekken, T.K.A., Henriques, J.C.C., Carrelhas, A.A.D., Gato, L.M.C.: Second order sliding mode control of oscillating water column wave energy converters for power improvement. IEEE Trans. Sustainable Energy 12(2), 1151–1160 (2021)
- Mosquera, F.D., Evangelista, C.A., Puleston, P.F., Ringwood, J.V.: Optimal wave energy extraction for oscillating water columns using second-order sliding mode control. IET Renew. Power Gener. 14(9), 1512–1519 (2020)
- Bartolini, G., Levant, A., Pisano, A., Usai, E.: Adaptive second-order sliding mode control with uncertainty compensation. Int. J. Control 89(9), 1747–1758 (2016)
- Shtessel, Y.B., Moreno, J.A., Fridman, L.: Twisting sliding mode control with adaptation: Lyapunov design, methodology and application. Automatica 75, 229–235 (2017)
- Utkin, V.I., Poznyak, A.S.: Adaptive sliding mode control with application to super-twist algorithm: Equivalent control method. Automatica 49(1), 39–47 (2013)



 Anderson, J.L., Moré, J.J., Puleston, P.F., Costa-Castelló, R.: Fuel cell module control based on switched/time-based adaptive super-twisting algorithm: Design and experimental validation. IEEE Trans. Control Syst. Technol. 31(1), 434–441 (2023)

- Wang, Y., Zhang, W., Zhang, Z., Cai, H.: Adaptive continuous sliding mode control of buck converters based on zero-crossing checking. In: IECON 2021–47th Annual Conference of the IEEE Industrial Electronics Society, pp. 1–5. IEEE, Piscataway (2021)
- Bartolini, G., Levant, A., Usai, E., Pisano, A.: 2-Sliding Mode with Adaptation. In: Proceedings of the 7th Mediterranean Conference on Control and Systems, pp. 2421–2429. IEEE, Piscataway (1999)
- Pisano, A., Tanelli, M., Ferrara, A.: Time-based switched sliding mode control for yaw rate regulation in two-wheeled vehicles. In: 2012 IEEE 51st IEEE Conference on Decision and Control (CDC), pp. 5028–5033. IEEE, Piscataway (2012)
- Capisani, L.M., Ferrara, A., Pisano, A.: Second-order sliding mode control with adaptive control authority for the tracking control of robotic manipulators. IFAC Proc. Vol. 44(1), 10319–10324 (2011)
- Evangelista, C.A., Pisano, A., Puleston, P., Usai, E.: Receding horizon adaptive second-order sliding mode control for doubly-fed induction generator based wind turbine. IEEE Trans. Control Syst. Technol. 25(1), 73–84 (2017)
- Evangelista, C., Pisano, A., Puleston, P., Usai, E.: Time-based adaptive second order sliding mode controller for wind energy conversion optimization. In: 53rd IEEE Conference on Decision and Control, pp. 2038–2043. IEEE, Piscataway (2014)
- Penalba, M., Ringwood, J.V.: A high-fidelity wave-to-wire model for wave energy converters. Renew. Energy 134, 367–378 (2019)
- Henriques, J.C.C., Portillo, J.C.C., Sheng, W., Gato, L.M.C., Falcão, A.F.O.: Dynamics and control of air turbines in oscillating-water-column wave energy converters: Analyses and case study. Renew. Sustainable Energy Rev. 112, 571–589 (2019)
- de O Falcão, A.F., Justino, P.A.P.: OWC wave energy devices with air flow control. Ocean Eng. 26(12), 1275–1295 (1999)
- Simonetti, I., Cappietti, L., Safti, H.E., Oumeraci, H.: Numerical modelling of fixed oscillating water column wave energy conversion devices: Toward geometry hydraulic optimization. In: Volume 9: Ocean Renewable Energy, pp. 1–10. American Society of Mechanical Engineers, New York (2015)
- 47. M'zoughi, F., Garrido, I., Garrido, A.J., De la Sen, M.: Fuzzy gain scheduled-sliding mode rotational speed control of an oscillating water column. IEEE Access, 8, 45853–45873 (2020)

- 48. Liu, Z., Xu, C., Qu, N., Cui, Y., Kim, K.: Overall performance evaluation of a model-scale owc wave energy converter. Renew. Energy 149, 1325–1338 (2020)
- Faÿ, F.X., Henriques, J.C., Kelly, J., Mueller, M., Abusara, M., Sheng, W., et al.: Comparative assessment of control strategies for the biradial turbine in the mutriku owc plant. Renew. Energy 146, 2766–2784 (2020)
- Mishra, S.K., Mohanta, D.K., Appasani, B., Kabalci, E.: OWC-Based Ocean Wave Energy Plants. Springer, Singapore (2020)
- M'zoughi, F., Garrido, A.J., Garrido, I., Bouallègue, S., Ayadi, M.: Sliding mode rotational speed control of an oscillating water column-based wave generation power plants. In: 2018 International Symposium on Power Electronics, Electrical Drives, Automation and Motion (SPEEDAM 2018), pp. 1263–1270. IEEE, Piscataway (2018)
- O'Sullivan, D.L., Lewis, A.W.: Generator selection and comparative performance in offshore oscillating water column ocean wave energy converters. IEEE Trans. Energy Convers. 26(2), 603–614 (2011)
- Sanchez, A., Molina, M., Lede, A.R.: Dynamic model of wind energy conversion systems with pmsg-based variable-speed wind turbines for power system studies. Int. J. Hydrogen Energy 37(13), 10064–10069 (2012)
- Ringwood, J.V., Bacelli, G., Fusco, F.: Energy-maximizing control of waveenergy converters: The development of control system technology to optimize their operation. IEEE CSM 34(5), 30–55 (2014)
- Trueworthy, A., DuPont, B.: The wave energy converter design process: Methods applied in industry and shortcomings of current practices. J. Marine Sci. Eng. 8(11) (2020)
- Vas, P.: Sensorless Vector and Direct Torque Control. Oxford University Press, New York (1998)
- 57. Utkin, V.I.: Sliding mode control design principles and applications to electric drives. IEEE Trans. Ind. Electron. 40(1), 23–36 (1993)
- Delavari, H., Ghaderi, R., Ranjbar, A., Momani, S.: Fuzzy fractional order sliding mode controller for nonlinear systems. Commun. Nonlinear Sci. Numer. Simul. 15(4), 963–978 (2010)

How to cite this article: Mosquera, F.D., Evangelista, C.A., Puleston, P.F., Ringwood, J.V.: Adaptive second order sliding mode control of an oscillating water column. IET Renew. Power Gener. 18, 226–237 (2024). https://doi.org/10.1049/rpg2.12912

